Homogeneity constraints on the mixed moments of velocity gradient and pressure Hessian in incompressible turbulence

Zhideng Zhou [1,2] and Ping-Fan Yang [1,2,3,*]

[1]*The State Key Laboratory of Nonlinear Mechanics, Institute of Mechanics, Chinese Academy of Sciences, Beijing 100190, China*
[2]*School of Engineering Sciences, University of Chinese Academy of Sciences, Beijing 100049, China*
[3]*Center for Combustion Energy and Department of Energy and Power Engineering, Tsinghua University, 100084 Beijing, China*

In homogeneous turbulent flow, a relation for the correlation between velocity gradient $m_{ij} \equiv \frac{\partial u_i}{\partial x_j}$ and pressure Hessian $h_{ij}^p \equiv \frac{\partial^2 p}{\partial x_i \partial x_j}$ was found recently: $\langle \mathrm{tr}(\mathbf{m}\mathbf{h^p}\mathbf{m}) \rangle = -\frac{1}{2} \langle (\mathrm{tr}(\mathbf{m}^2))^2 \rangle$. We discuss the implications of this relation to the velocity gradient dynamics: together with the Poisson equation for pressure, the homogeneity relation yields an identity between $\langle (\mathrm{tr}(\mathbf{m}^2))^2 \rangle$ and the integration of a two-point fourth-order correlation function of velocity gradient for isotropic flows. Our results indicate that the main contributions to $\langle \mathrm{tr}(\mathbf{m}\mathbf{h^p}\mathbf{m}) \rangle$ come from scales less than roughly 20 times the Kolmogorov scale. Also, the homogeneity relation provides restrictions to the parameters in the closure models of pressure Hessian in velocity gradient dynamics. We further discuss the generalization of this homogeneity relation to turbulent shear flows, and we show numerically that this relation between $\langle \mathrm{tr}(\mathbf{m}\mathbf{h^p}\mathbf{m}) \rangle$ and $\langle (\mathrm{tr}(\mathbf{m}^2))^2 \rangle$ is approximately satisfied even in the presence of a shear and of a wall, as it occurs in turbulent channel flows.

I. INTRODUCTION

The velocity gradient $m_{ij} \equiv \frac{\partial u_i}{\partial x_j}$ is an essential quantity for understanding the small-scale properties of turbulence. It contains rich information on the local structures of turbulent flows. For example, the turbulent dissipation rate ε is directly related to the second-order moments of velocity gradient $\varepsilon = 2\nu \langle s_{ij} s_{ji} \rangle$, where $\mathbf{s}$ is the rate of strain tensor defined as $s_{ij} \equiv (m_{ij} + m_{ji})/2$. When studying the dynamics of the second-order moments of $\mathbf{m}$, the third-order moments of $\mathbf{m}$ appear due to the nonlinearity of the Navier-Stokes equation. For example, the vortex stretching term $\langle \omega_i s_{ij} \omega_j \rangle$ appears in the evolution equation of enstrophy $\langle \omega_i \omega_i \rangle$. Here ω_i is the vorticity vector defined as $\omega_i \equiv -\epsilon_{ijk} w_{jk}$, where ϵ_{ijk} is the Levi-Civita symbol and $w_{jk} \equiv (m_{jk} - m_{kj})/2$. In his classical paper [1], Betchov derived two kinematic constraints on the second- and third-order moments of $\mathbf{m}$ for homogeneous flows:

$$\langle \overline{\mathbf{m}^2} \rangle = \langle \overline{\mathbf{m}^3} \rangle = 0, \tag{1}$$

where we use the overbar symbol to denote the trace operation $\mathrm{tr}(\cdot)$ for simplicity. These equalities result from the homogeneity condition and the chain rule of derivatives, which provide further insights into the statistics of $\mathbf{m}$ [2,3]. For instance, $\langle \overline{\mathbf{m}^3} \rangle = 0$ and the positive vortex stretching implies that the intermediate eigenvalue of strain is preferentially positive [1,4].

---

*Corresponding author: yangpingfan@imech.ac.cn

When studying the second-order moments of $\mathbf{m}$, the pressure Hessian tensor $h_{ij}^p \equiv \frac{\partial^2 p}{\partial x_i \partial x_j}$ does not appear explicitly in the dynamic equations since $\langle h_{ij}^p m_{ij} \rangle = 0$ due to homogeneity [4]. On the other hand, if we consider the equation of third-order moments of $\mathbf{m}$, both the nonlinear fourth-order moments and the mixed moments between pressure Hessian and velocity gradient are nonzero [cf. the ensemble average of Eqs. (C23) and (C24) of Ref. [4]]. The studies of fourth-order moments of $\mathbf{m}$ were initiated by Siggia [5], where the author managed to express all the fourth-order moments in terms of four independent fourth-order invariants of $\mathbf{m}$. Later Hierro and Dopazo [6] extended the discussions to the general expressions of fourth-order moments of $\mathbf{m}$. Various theoretical and numerical studies have been devoted to the fourth-order derivatives and invariants [7–11] and even higher-order moments [12]. On the other hand, although many people have investigated the properties of pressure Hessian, especially for the dynamic model of velocity gradient [13–17], and also the implications from Poisson equation [18], less attention has been paid to the mixed invariants appearing in the third-order equations, except the early work by Tsinober *et al.* [19]. Also, with the aim of designing closure models for velocity gradient dynamics, the pressure and viscosity terms have been investigated by using different assumptions and models, respectively. Under these approximations, modeling results are in good agreement with observations from direct numerical simulation (DNS), with a special focus on the second- and third-order invariants of the anisotropic (traceless) portion of the velocity gradient tensor. However, those assumptions and models for the pressure and viscosity terms are intrinsically inexact and might violate some mathematical constraints. Recently, Fang *et al.* [9] found that the relation of fourth-order invariants in compressible homogeneous isotropic turbulence (HIT) is similar to incompressible HIT, which can be approached by a linear model of Gaussian and restricted Euler states. This model is also phenomenological and not an exact relation. Very recently, using tensor function representation theory, Carbone and Wilczek [20] found a relation between the fourth-order moment $\langle (\overline{\mathbf{m}^2})^2 \rangle$ and the mixed moment $\langle \overline{\mathbf{m} \mathbf{h}^\mathbf{p} \mathbf{m}} \rangle$ for isotropic flows. As we show in this work, this relation can help us to better understand the statistical properties of pressure Hessian, as it is the case for Betchov's relations to the velocity gradient. In Sec. II we will review the dynamic equations of the moments of $\mathbf{m}$, and from which we could see that the homogeneity condition not only leads to constraints on the second- and third-order moments, but also results in an identity between $\langle (\overline{\mathbf{m}^2})^2 \rangle$ and $\langle \overline{\mathbf{m} \mathbf{h}^\mathbf{p} \mathbf{m}} \rangle$. Next in Sec. III we will investigate the implications of the Poisson equation for pressure to homogeneity relation discussed in Sec. II. In Sec. IV we will discuss the implication of this invariant's relation to the velocity gradient models. And, finally, in Sec. V we will generalize the discussions to the anisotropic shear flows.

II. DYNAMIC EQUATIONS AND THE HOMOGENEITY CONSTRAINTS ON THE INVARIANTS OF m

In this section, we first discuss the invariant's equations of the velocity gradient tensor $m_{ij} = \frac{\partial u_i}{\partial x_j}$. Starting from the incompressible Navier-Stokes equation

$$\frac{\partial u_i}{\partial t} + u_j \nabla_j u_i = -\nabla_i p + \nu \nabla^2 u_i, \tag{2}$$

we could readily derive the evolution equations for the invariants of $\mathbf{m}$, namely, $Q \equiv -\frac{1}{2}\overline{\mathbf{m}^2}$ and $R \equiv -\frac{1}{3}\overline{\mathbf{m}^3}$ [21]:

$$\frac{dQ}{dt} = -3R - m_{ij}H_{ji}, \tag{3}$$

$$\frac{dR}{dt} = \frac{2}{3}Q^2 - m_{ij}m_{jk}H_{ki}, \tag{4}$$

where $\mathbf{H}$ denotes $H_{ij} \equiv -(\frac{\partial^2 p}{\partial x_i \partial x_j} - \frac{\partial^2 p}{\partial x_k \partial x_k}\frac{\delta_{ij}}{3}) + \nu \frac{\partial^2 A_{ij}}{\partial x_k \partial x_k}$, as defined in Ref. [21]. For convenience, we denote H_{ij}^p and H_{ij}^ν as the pressure and viscous parts of the tensor $\mathbf{H}$. Now taking the ensemble averages of Eqs. (3) and (4), then for steady-state flows, the various terms on the right-hand side of Eqs. (3) and (4) should balance with each other, i.e.,

$$-3\langle R \rangle - \langle m_{ij} H_{ji} \rangle = 0, \tag{5}$$

$$\tfrac{2}{3}\langle Q^2 \rangle - \langle m_{ij} m_{jk} H_{ki} \rangle = 0. \tag{6}$$

According to Eq. (1), $\langle Q \rangle = \langle R \rangle = 0$ in incompressible homogeneous flows. Actually, Eq. (1) could be generalized to more general cases: for any vector fields $\mathbf{a}$, $\mathbf{b}$, $\mathbf{c}$ and their spatial gradient fields $\mathbf{h^a} = \nabla \mathbf{a}$, $\mathbf{h^b} = \nabla \mathbf{b}$, $\mathbf{h^c} = \nabla \mathbf{c}$, we have proven that [22]

$$\langle \overline{\mathbf{h^a} \mathbf{h^b}} \rangle = \langle \overline{\mathbf{h^a}} \, \overline{\mathbf{h^b}} \rangle, \tag{7}$$

$$\langle \overline{\mathbf{h^a} \mathbf{h^b} \mathbf{h^c}} \rangle + \langle \overline{\mathbf{h^a} \mathbf{h^c} \mathbf{h^b}} \rangle = \langle \overline{\mathbf{h^a} \mathbf{h^b}} \, \overline{\mathbf{h^c}} \rangle + \langle \overline{\mathbf{h^b} \mathbf{h^c}} \, \overline{\mathbf{h^a}} \rangle + \langle \overline{\mathbf{h^c} \mathbf{h^a}} \, \overline{\mathbf{h^b}} \rangle - \langle \overline{\mathbf{h^a}} \, \overline{\mathbf{h^b}} \, \overline{\mathbf{h^c}} \rangle. \tag{8}$$

If we choose $a_i = b_i = c_i = u_i$, Eqs. (7) and (8) reduce to Eq. (1). On the other hand, it is obvious that the viscous terms $\langle \overline{\mathbf{m} \mathbf{H}^\nu} \rangle$ and $\langle \overline{\mathbf{m}^2 \mathbf{H}^\nu} \rangle$ are also zero if we choose $a_i = c_i = u_i$ and $b_i = \nabla^2 u_i$ in Eqs. (7) and (8). Then, in order to satisfy Eqs. (5) and (6), we should have

$$\langle m_{ij} H_{ji}^p \rangle = 0, \tag{9}$$

$$\langle \tfrac{2}{3} Q^2 \rangle = \langle m_{ij} m_{jk} H_{ki}^p \rangle, \tag{10}$$

which could also be derived from the homogeneity condition, as we will show in the following. In Eqs. (7) and (8), if we choose $a_i = c_i = u_i$ and $b_i = \frac{\partial p}{\partial x_i}$, Eq. (9) is readily proven from Eq. (7), and Eq. (8) reduces to

$$\left\langle \frac{\partial u_i}{\partial x_j} \frac{\partial u_j}{\partial x_i} \frac{\partial^2 p}{\partial x_k \partial x_k} \right\rangle = 2 \left\langle \frac{\partial u_i}{\partial x_j} \frac{\partial^2 p}{\partial x_j \partial x_k} \frac{\partial u_k}{\partial x_i} \right\rangle. \tag{11}$$

Notice that $\frac{\partial^2 p}{\partial x_k \partial x_k} = -\mathrm{tr}(\mathbf{m}^2)$, Thus,

$$\left\langle m_{ij} \frac{\partial^2 p}{\partial x_j \partial x_k} m_{ki} \right\rangle = \langle \overline{\mathbf{m} \mathbf{h^p} \mathbf{m}} \rangle = -\frac{1}{2}\langle \overline{(\mathbf{m}^2)^2} \rangle = -\langle \overline{\mathbf{m}^4} \rangle, \tag{12}$$

and the last equality holds as a result of Cayley-Hamilton theorem. Now we show that Eq. (10) is tantamount to Eq. (12). Recall the definition of $\mathbf{H^p}$, $\mathbf{H^p} = -\mathbf{h^p} + \frac{1}{3}\overline{\mathbf{h^p}}\mathbf{I}$, which is the deviatoric part of pressure Hessian and related to the velocity gradient at the other locations via the Poisson equation (see Sec. III for detail discussions). From Eq. (12), we have

$$\langle m_{ij} H_{jk}^p m_{ki} \rangle = \left\langle m_{ij} \left(-\frac{\partial^2 p}{\partial x_j \partial x_k} \right) m_{ki} \right\rangle + \left\langle m_{ij} \left(\frac{1}{3} \frac{\partial^2 p}{\partial x_m \partial x_m} \delta_{jk} \right) m_{ki} \right\rangle$$

$$= \frac{1}{2}\langle \overline{(\mathbf{m}^2)} \rangle - \frac{1}{3}\langle \overline{(\mathbf{m}^2)} \rangle = \frac{1}{6}\langle \overline{(\mathbf{m}^2)} \rangle = \left\langle \frac{2}{3} Q^2 \right\rangle, \tag{13}$$

which is exactly Eq. (10). Here we remind that Eq. (12) is first obtained in Ref. [20] by tensor function representation theory for isotropic flows, and the derivation here releases the condition to only homogeneity. Notice that $\langle \frac{2}{3} Q^2 \rangle$ is directly related to the fourth-order moments of $\mathbf{m}$ [5,8]:

$$\left\langle \tfrac{2}{3} Q^2 \right\rangle = \tfrac{1}{6}\langle (m_{ij} m_{ji})^2 \rangle = \tfrac{1}{6}(I_1 - I_2 + I_4/4), \tag{14}$$

where we denote $I_1 \equiv \langle (\overline{\mathbf{s^2}})^2 \rangle$, $I_2 \equiv \langle \overline{\mathbf{s^2} \, \boldsymbol{\omega}^2} \rangle$, and $I_4 \equiv \langle (\boldsymbol{\omega}^2)^2 \rangle$. Together with the quantity $I_3 \equiv \langle \boldsymbol{\omega} \cdot \mathbf{s}^2 \cdot \boldsymbol{\omega} \rangle$, they represent the four independent fourth-order invariants of velocity gradient, from which

TABLE I. A list of our HIT data sets showing the Reynolds number R_λ, the number of grid points N in the three spatial directions in DNS, and the number of statistics we use in the calculations of this work.

Case	R129	R433	R610	R610h	R1300
R_λ	129	433	610	610	1300
N	512	1024	4096	8192	8192
Points	2.68×10^9	2.68×10^8	1.34×10^8	1.34×10^8	1.34×10^8

we can determine all components of fourth-order moments of velocity gradient in homogeneous and isotropic turbulence [5].

Now we verify Eq. (12) by DNS data. First, we briefly introduce the DNS cases of HIT used in this work. In Table I we list and label all the DNS cases, including case R129, a simulation of HIT performed by the authors with 512^3 grids and the Taylor-scale Reynolds numbers $R_\lambda = 129$, this DNS is performed using a standard pseudospectral method covering a periodic box of side $L = 2\pi$ (see Refs. [23,24] for more details). We used 20 snapshots resulting in $20 \times 512^3 = 2.68 \times 10^9$ data points. The other four cases are all from the Johns Hopkins Turbulence Database (JHTDB). Case R433 comes from the data set "Forced isotropic turbulence" with 1024^3 grids and $R_\lambda = 433$ [25]. We downloaded 64 snapshots, equally distributed over the simulation duration, with each snapshot $128 \times 128 \times 256$ data points, resulting in 2.68×10^8 data points in total. Case R610 comes from the "Forced isotropic turbulence data set on 4096^3 Grid" data set [26] with 4096^3 grids and $R_\lambda = 610$. Cases R610h and R1300 come from the snapshots 5 and 3 of the "Forced isotropic turbulence data set on 8192^3 Grid" data set [27,28] with 8192^3 grids and $R_\lambda = 610$ and 1300, respectively. For cases R610, R610h, and R1300, we downloaded $512^3 = 1.34 \times 10^8$ data points from one single snapshot. In Table II we use cases R433, R610h, and R1300 to check Eq. (12): those results agree well with Eq. (12) and thus verify the main result of this section.

III. IMPLICATIONS FROM THE POISSON EQUATION FOR PRESSURE

In the previous section, we discuss the dynamic equations of the velocity gradient and the homogeneity constraint to the third-order mixed moments of velocity gradient and pressure Hessian. As we mentioned previously, the deviatoric part of pressure Hessian H_{ij}^p is nonlocal and relates to the velocity gradient tensor at the other locations via the Poisson equation [cf. Eqs. (28)– (31) of Ref. [29] or classical textbooks like Ref. [30]]:

$$H_{ij}^p(\mathbf{x}) = \frac{1}{4\pi} \int d\mathbf{x}' \left[\frac{\delta_{ij}}{|\mathbf{x} - \mathbf{x}'|^3} - 3\frac{(\mathbf{x} - \mathbf{x}')_i (\mathbf{x} - \mathbf{x}')_j}{|\mathbf{x} - \mathbf{x}'|^5} \right] \times m_{ln} m_{nl}(\mathbf{x}'). \tag{15}$$

TABLE II. Results for the mixed moment $\langle \overline{\mathbf{mh^p m}} \rangle$ and the fourth-order moment $\frac{1}{2} \langle (\mathbf{m}^2)^2 \rangle$ normalized by $\langle \mathbf{s}^2 \rangle^2$ from DNS data with $R_\lambda = 433$, 610, and 1300.

Case	R433	R610h	R1300
$\langle \overline{\mathbf{mh^p m}} \rangle / \langle \mathbf{s}^2 \rangle^2$	−2.35	−2.80	−3.71
$\frac{1}{2} \langle (\mathbf{m}^2)^2 \rangle / \langle \mathbf{s}^2 \rangle^2$	2.35	2.81	3.70

Therefore, applying the above equation to the expression of the mixed third-order moments would help us to understand its nonlocal properties. Plugging Eq. (15) to $\langle \overline{\mathbf{mH^p m}} \rangle$ yields

$$\langle m_{ij} m_{jk} H_{ki}^p \rangle = \frac{1}{4\pi} \int d\mathbf{x'} \left[\frac{\delta_{ki}}{|\mathbf{x} - \mathbf{x'}|^3} - 3\frac{(\mathbf{x} - \mathbf{x'})_i (\mathbf{x} - \mathbf{x'})_k}{|\mathbf{x} - \mathbf{x'}|^5} \right] \langle m_{ln} m_{nl}(\mathbf{x'}) m_{ij} m_{jk}(\mathbf{x}) \rangle$$

$$= \frac{1}{4\pi} \int d\mathbf{r} \left[\frac{\delta_{ki}}{r^3} - 3\frac{r_i r_k}{r^5} \right] \langle m_{ln} m_{nl}(0) m_{ij} m_{jk}(\mathbf{r}) \rangle, \tag{16}$$

where $\mathbf{r} \equiv \mathbf{x} - \mathbf{x'}$. We denote $K_{ik}(\mathbf{r}) \equiv \langle m_{ln} m_{nl}(0) m_{ij} m_{jk}(\mathbf{r}) \rangle$ and it is a second-rank tensor function depended on $\mathbf{r}$, therefore in isotropic flows, it could be expressed as

$$K_{ik}(\mathbf{r}) = \frac{K_1(r)}{r^2} r_i r_k + K_2(r) \delta_{ik}, \tag{17}$$

where we define

$$K_1(r) \equiv K_{LL}(r) - K_{NN}(r), \tag{18}$$

$$K_2(r) \equiv K_{NN}(r), \tag{19}$$

here $K_{LL}(r)$ and $K_{NN}(r)$ are the projections of K_{ij} parallel and orthogonal to $\mathbf{r}$, respectively:

$$K_{LL}(r) \equiv \langle m_{ln} m_{nl}(0) m_{Lj} m_{jL}(r) \rangle, \tag{20}$$

$$K_{NN}(r) \equiv \langle m_{ln} m_{nl}(0) m_{Nj} m_{jN}(r) \rangle, \tag{21}$$

and the subscripts L and N refer to the longitudinal and transverse directions, respectively. Then, we have

$$\langle m_{ij} m_{jk} H_{ki}^p \rangle = \int_0^\infty r^2 dr \left[\frac{\delta_{ki}}{r^3} - 3\frac{r_i r_k}{r^5} \right] \left(\frac{K_1(r)}{r^2} r_i r_k + K_2(r) \delta_{ik} \right)$$

$$= -2 \int_0^\infty \frac{K_1(r)}{r} dr. \tag{22}$$

Also notice that $K_{ii}(0) = K_1(0) + 3K_2(0) = \langle (m_{ij} m_{ji})^2 \rangle$ and $K_1(0) = 0$ due to isotropy, which yields

$$K_2(0) = \frac{1}{3} \langle (\overline{\mathbf{m}^2})^2 \rangle = -4 \int_0^\infty \frac{K_1(r)}{r} dr. \tag{23}$$

For isotropic flows, it is easy to see that $K_1(0) = 0$ from Eq. (18). And since $K_1(r)$ is an even function, the linear term in the Taylor expansion of $K_1(r)$ vanishes and $K_1(r) \sim r^2$ at $r = 0$, thus, $K_1(r)/r = 0$ at $r = 0$. Therefore, the integrand of Eq. (22) vanishes at $r = 0$ and we can conclude that the term $\langle m_{ij} m_{jk} H_{ki}^p \rangle$ originates fully from the nonlocal contributions of the integrand.

In Fig. 1 we plot the functions of $K_{LL}(r)$, $K_{NN}(r)$, and $\frac{K_1(r)}{r}$ normalized by $\langle \overline{\mathbf{m}^4} \rangle$ and η extracted from the DNS, where we use data from cases R129, R610, R610h, and R1300. From Fig. 1 one can see that those curves collapse well for $R_\lambda = 610$ and 1300, and for the two different resolutions of $R_\lambda = 610$. The low Reynolds number results of $R_\lambda = 129$ deviate from the two higher Reynolds numbers, possibly due to the finite Reynolds number effect. Because of the resolution of JHTDB, we lack the data points in the range of small r for $R_\lambda = 610$ and 1300, which are supplemented by the $R_\lambda = 129$ case, one can see that $K_1(r)/r$ indeed decreases to 0 as $r \to 0$. On the other hand, the curves of $K_1(r)/r$ for all Reynolds numbers peak at about 3η. Therefore, although the integrand $K_1(r)/r = 0$ at $r = 0$, the term $\langle m_{ij} m_{jk} H_{ki}^p \rangle$ is still a dissipative range quantity. A preliminary understanding of this behavior would be applying the quasinormal (q.n.) assumption to the two-point fourth-order velocity gradient correlations in the integration expression of $\langle \overline{\mathbf{mH^p m}} \rangle$ [Eq. (16)], we find that the q.n. expression of K_1 catches the shape of the curves in Fig. 1, although the values are
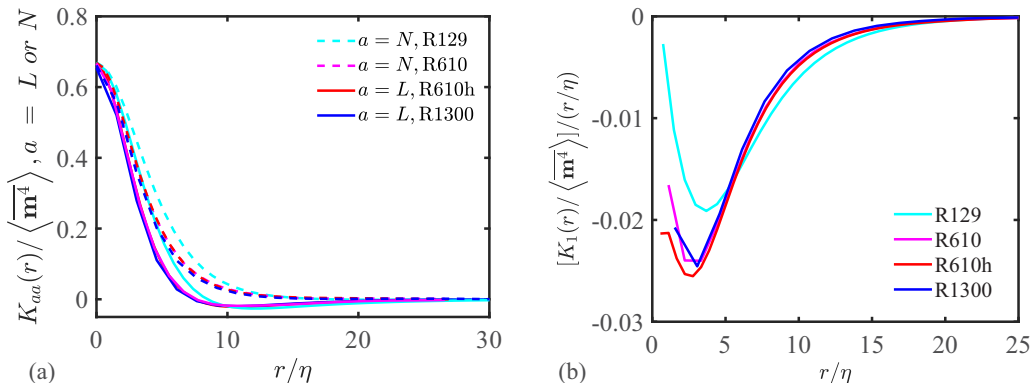
FIG. 1. (a) $K_{LL}(r)$ (solid lines) and $K_{NN}(r)$ (dashed lines) normalized by $\langle \overline{\mathbf{m}^4} \rangle$ vs r/η and (b) $\frac{K_1(r)}{r}$ normalized by $\langle \overline{\mathbf{m}^4} \rangle / \eta$ vs r/η. The cyan, magenta, red, and blue lines indicate cases R129, R610, R610h, and R1300, respectively.

much smaller. In Appendix A we give detailed discussions on the application of q.n. assumption to some of the quantities and expressions that appeared in the main text.

IV. IMPLICATIONS FOR PARAMETERS IN THE VELOCITY GRADIENT MODELS

In Sec. II we derived the following equation [Eq. (13)]:

$$\langle m_{ij} m_{jk} H^p_{ki} \rangle = \tfrac{1}{6} \langle (m_{ij} m_{ji})^2 \rangle. \tag{24}$$

In this section, we discuss the implications of this identity to the closure models of velocity gradient dynamics. Borue and Orszag [31] have argued that for the coarse-grained field, the deviatoric part of pressure Hessian is approximately proportional to the deviatoric part of $\mathbf{m}^2$: $\mathbf{H^p} \propto \mathbf{m}^2 - \frac{1}{3}\overline{\mathbf{m}^2}\mathbf{I}$ [cf. Eq. (5.18) of Ref. [31]]. Inspired by this observation, Chertkov et al. [32] proposed the tetrad's model for the (perceived) velocity gradient:

$$H^p_{ij} \equiv -\left(\frac{\partial^2 p}{\partial x_i \partial x_j} - \frac{\partial^2 p}{\partial x_k \partial x_k} \frac{\delta_{ij}}{3} \right) = \alpha \left(m_{ik} m_{kj} - \frac{1}{3}\overline{\mathbf{m}^2}\delta_{ij} \right), \tag{25}$$

plugging it into Eq. (24) yields

$$\tfrac{1}{6} \langle (\overline{\mathbf{m}^2})^2 \rangle = \langle m_{ij} m_{jk} H^p_{ki} \rangle = \alpha \left(\langle \overline{\mathbf{m}^4} \rangle - \tfrac{1}{3} \langle (\overline{\mathbf{m}^2})^2 \rangle \right) = \frac{\alpha}{6} \langle (\overline{\mathbf{m}^2})^2 \rangle, \tag{26}$$

which gives $\alpha = 1$. Following Fig. 17(c) of Ref. [31], in Fig. 2 we plot the joint probability density function (PDF) between $\frac{2}{3}Q^2$ and $\overline{\mathbf{m}^2\mathbf{H^p}}$ normalized by their mean values, where we use data from case R1300. We can see that the conditional mean $\langle \overline{\mathbf{m}^2\mathbf{H^p}} | \frac{2}{3}Q^2 \rangle$ is very close to a straight line with slope 1, which is consistent with $\alpha = 1$ in Eq. (26) above. On the other hand, we should remind that the homogeneity relation (24) is a scalar relation and only constitutes projections of the pressure Hessian along particular directions, while Eq. (25) is a tensor model with five independent components, thus Eq. (24) could not fully measure the quality of the closure model for pressure Hessian. Recently Wilczek and Meneveau [14] introduced the Gaussian closure for pressure Hessian in velocity gradient dynamics, which could be regarded as a generalization of Eq. (25):

$$-H^p_{ij} = \alpha \left(s_{ik} s_{kj} - \tfrac{1}{3}\overline{\mathbf{s}^2}\delta_{ij} \right) + \beta \left(w_{ik} w_{kj} - \tfrac{1}{3}\overline{\mathbf{w}^2}\delta_{ij} \right) + \gamma (s_{ik} w_{kj} - w_{ik} s_{kj}), \tag{27}$$
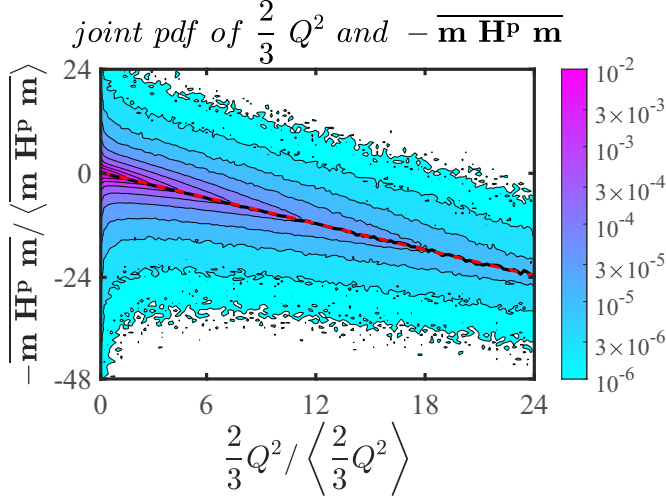
FIG. 2. Joint PDF between $\frac{2}{3}Q^2$ and $\overline{\mathbf{m^2 H^p}}$ normalized by their mean values. The black solid line is the conditional mean $\langle \overline{\mathbf{m^2 H^p}} | \frac{2}{3}Q^2 \rangle$ and the red dashed line is a straight line with slope 1. Data come from case R1300 of HIT.

where α, β, and γ are model parameters. Plugging Eq. (27) into Eq. (24) yields

$$\langle m_{ij} m_{jk} H_{ki}^p \rangle = -\frac{\alpha}{6} I_1 + \frac{\alpha + \beta}{12} I_2 - \frac{\alpha + \beta}{4} I_3 - \frac{\beta}{24} I_4. \tag{28}$$

Table III gives the values of mixed moment $\langle \overline{\mathbf{mH^p m}} \rangle$ and the fourth-order invariants I's normalized by I_1 extracted from DNS of three different R_λ as in Table II, and also the value $I_1/\langle \overline{\mathbf{s^2}} \rangle^2$ for reference. One can see that all the ratios in Table III are roughly constants with respect to Reynolds number, consistent with the observations in Ref. [8]. We could choose $I_2/I_1 \approx 1.73$, $I_3/I_1 \approx 0.24$, $I_4/I_1 \approx 8.1$, $\langle \overline{\mathbf{mH^p m}} \rangle / I_1 \approx 0.21$, and plug those values into Eq. (28), which yields a quantitative relation between the parameters α and β:

$$\beta = -0.829 - 0.326\alpha. \tag{29}$$

In Ref. [14], based on the assumption of Gaussian velocity fields, one could theoretically calculate the values of model parameters: $\alpha = -\frac{2}{7}$ and $\beta = -\frac{2}{5}$. Plugging these two values into Eq. (29) leads to an 80% error between the left-hand side and right-hand side of the equation, showing that the Gaussian closure approach violates the homogeneity constraint when the velocity gradients are not Gaussian but belong to a turbulent ensemble. On the other hand, we remind that there exist specific values of α and β which generate Gaussian and homogeneous ensemble for velocity gradient [33], and in this case we expect those homogeneity constraints are fulfilled.

TABLE III. Results for the mixed moment $\langle \overline{\mathbf{mH^p m}} \rangle$ and the fourth-order moments of velocity gradient I_2 to I_4 normalized by I_1 from DNS of $R_\lambda = 433$, 610, and 1300. We also show the values $I_1/\langle \overline{\mathbf{s^2}} \rangle^2$ for reference.

	$I_1/\langle \overline{\mathbf{s^2}} \rangle^2$	I_2/I_1	I_3/I_1	I_4/I_1	$\langle \overline{\mathbf{mH^p m}} \rangle / I_1$
R433	3.58	1.71	0.248	8.07	0.211
R610h	4.50	1.75	0.236	7.98	0.208
R1300	5.60	1.73	0.245	8.18	0.214

In addition to the Gaussian closure, Ref. [14] also estimated the parameters from DNS data. Contracting Eq. (27) with $\mathbf{sw}$, $\mathbf{s}^2$, and $\mathbf{w}^2$, respectively, and taking the ensemble average would give three identities for the three parameters α, β, γ [see Eqs. (4.13) to (4.15) in Ref. [14]]. Extracting those coefficients from DNS, one could determine $\alpha = -0.61$ and $\beta = -0.65$ [14]. This approach is called the "enhanced Gaussian closure" in Ref. [14], and since $\mathbf{m}^2 = \mathbf{s}^2 + \mathbf{w}^2 + \mathbf{sw} + \mathbf{ws}$, this approach is consistent with the homogeneity constraint (24). Plugging these two values $\alpha = -0.61$ and $\beta = -0.65$ into Eq. (29), the errors between the left- and right-hand sides are only 3%, showing that the enhanced Gaussian closure indeed agrees with the homogeneity constraint. Table III also suggests that Eq. (29) is approximately Reynolds number independent.

At this point, the reader might raise the question whether homogeneity constraints with order higher than Eq. (24) exist and provide further constraints to the closure model. In Appendix B we show that although we could derive a relation similar to Eq. (8) for the fourth-order moments [Eq. (B1)], it is not an independent constraint imposed by the homogeneity condition and could be derived from pure mathematical tensor relations. One might prove that homogeneity does not lead to further constraint by tensor function representation theory [20], but this is beyond the scope of this work.

V. GENERALIZATION TO THE TURBULENT SHEAR FLOWS

In this section, we discuss the generalization of Eq. (12) to turbulent shear flows. The motivation is that although the Betchov relations [Eq. (1)] require homogeneity condition, they hold approximately even in the log-layer and bulk region of turbulent boundary layer [34,35]. Thus, it would be interesting to see whether the homogeneity constraint for pressure Hessian derived in Sec. II works in the presence of a shear and a wall. First we notice that Eq. (12) should be modified when the flow possesses a mean velocity gradient since in this case, the Poisson equation becomes

$$\frac{\partial^2 p}{\partial x_k \partial x_k} = -\overline{\mathbf{m}^2} - 2\overline{\mathbf{mM}} + \langle \overline{\mathbf{m}^2} \rangle, \tag{30}$$

where $\mathbf{M}$ denotes the mean gradient $M_{ij} = \frac{\partial \langle U_i \rangle}{\partial x_j}$. Plugging Eq. (30) into Eq. (11) yields

$$\langle \overline{\mathbf{mh^p m}} \rangle = -\tfrac{1}{2}\big(\langle (\overline{\mathbf{m}^2})^2 \rangle + 2\langle \overline{\mathbf{m}^2} m_{ij} \rangle M_{ji} - \langle \overline{\mathbf{m}^2} \rangle^2 \big). \tag{31}$$

Notice that in homogeneous flows $\langle \overline{\mathbf{m}^2} \rangle = 0$ and thus the last term on the right-hand side of Eq. (31) vanishes. Even in turbulent boundary layers, experimental and DNS data show that $\langle \overline{\mathbf{m}^2} \rangle \ll \langle \overline{\mathbf{s}^2} \rangle$ [34,35], so one could expect that the last term on the right-hand side of Eq. (31) is negligible in these cases. Now considering the second term on the right-hand side of Eq. (31), $\langle \overline{\mathbf{m}^2} m_{ij} \rangle M_{ji}$, we could show that for high Reynolds number homogeneous shear flows (HSF), this term is much smaller than $\langle (\overline{\mathbf{m}^2})^2 \rangle$, which is the first term on the right-hand side of Eq. (31), thus, in this case Eq. (31) reduces to Eq. (12). The arguments are the following: we first denote x_1 and x_2 as the coordinates in the streamwise and normal directions, and in HSF, the only nonvanishing component of the mean gradient M_{ij} is M_{12}. As a result, $\langle \overline{\mathbf{m}^2} m_{ij} \rangle M_{ji} = \langle \overline{\mathbf{m}^2} m_{21} \rangle M_{12} = \langle m_{ij} m_{ji} m_{21} \rangle M_{12}$. Then we notice that i and j in $\langle m_{ij} m_{ji} m_{21} \rangle$ are both repeated indices, thus, all the individual terms forming $\langle m_{ij} m_{ji} m_{21} \rangle$, like $\langle m_{12} m_{21} m_{21} \rangle$ and $\langle m_{13} m_{31} m_{21} \rangle$, etc., must have odd numbers of 1 and 2 among all the indices. According to the analysis in Ref. [36], the odd components of the third-order moments of velocity gradient scale with Reynolds number as $\propto R_\lambda^{-1/2}$ when normalized by $\langle \overline{\mathbf{s}^3} \rangle$, where $R_\lambda = \langle u_1^2 \rangle / (\nu \langle (\frac{\partial u_1}{\partial x_1})^2 \rangle^{1/2})$ is the Reynolds number based on the Taylor microscale by using the velocity fluctuation and its derivative along the streamwise direction x_1. That means we expect $\langle m_{ij} m_{ji} m_{21} \rangle \sim \langle \overline{\mathbf{s}^3} \rangle R_\lambda^{-1/2}$. Furthermore, the mean gradient M_{12} is much smaller than the fluctuation $\langle (\frac{\partial u_1}{\partial x_1})^2 \rangle^{1/2}$ when R_λ is large, as we show below. The mean gradient scales as $M_{12} \sim \frac{\langle u_1^2 \rangle^{1/2}}{L}$, where L is the characteristic length scale of the system. The second-order moment of the velocity gradient
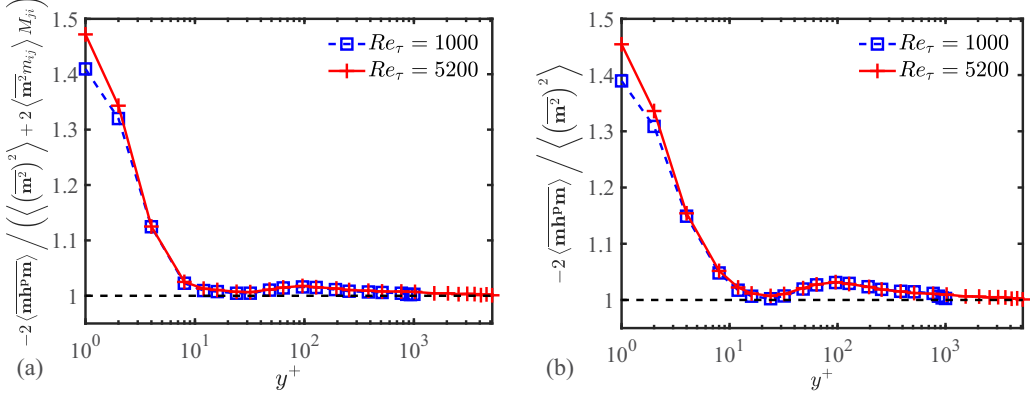
FIG. 3. (a) The ratio $-2\langle\overline{\mathbf{mh^p m}}\rangle/(\langle(\overline{\mathbf{m}^2})^2\rangle + 2\langle\overline{\mathbf{m}^2}m_{ij}\rangle M_{ji})$ in channel flows. For homogeneous flows, those values should be 1. The red solid line with plus symbols indicates the $\mathrm{Re}_\tau = 5200$ case, while the blue dashed line with square symbols indicates the $\mathrm{Re}_\tau = 1000$ case. (b) $-2\langle\overline{\mathbf{mh^p m}}\rangle/\langle(\overline{\mathbf{m}^2})^2\rangle$ in channel flows for comparison. The black dashed line indicates the value 1, the corresponding value for homogeneous flows.

$\frac{\partial u_1}{\partial x_1}$ scales as $\langle(\frac{\partial u_1}{\partial x_1})^2\rangle \sim \frac{\varepsilon}{\nu} \sim \frac{\langle u_1^2\rangle^2}{R_\lambda^2 \nu^2}$, where we use $R_\lambda = \frac{\langle u_1^2\rangle^{1/2}\lambda}{\nu}$ and $\lambda/\langle u_1^2\rangle^{1/2} \sim (\nu/\varepsilon)^{1/2}$, λ is the Taylor microscale [37]. Thus, $M_{12}/\langle(\frac{\partial u_1}{\partial x_1})^2\rangle^{1/2} \sim \frac{\langle u_1^2\rangle^{1/2}}{L} \times \frac{R_\lambda\nu}{\langle u_1^2\rangle} \sim R_\lambda/\mathrm{Re} \sim R_\lambda^{-1}$, in the last step we use $\mathrm{Re} = \langle u_1^2\rangle^{1/2}L/\nu \sim R_\lambda^2$ [37]. On the other hand, DNS data of HIT show that the skewness and flatness of the velocity gradient scale as $\langle(\frac{\partial u_1}{\partial x_1})^3\rangle/\langle(\frac{\partial u_1}{\partial x_1})^2\rangle^{3/2} \sim R_\lambda^{0.1}$ and $\langle(\frac{\partial u_1}{\partial x_1})^4\rangle/\langle(\frac{\partial u_1}{\partial x_1})^2\rangle^2 \sim R_\lambda^{0.3}$ [8]. Therefore, we estimate that $\langle\overline{\mathbf{m}^2}m_{21}\rangle M_{12} \sim (\langle\overline{\mathbf{s}^3}\rangle R_\lambda^{-1/2}) \times (\langle(\frac{\partial u_1}{\partial x_1})^2\rangle^{1/2}R_\lambda^{-1}) \sim \langle(\frac{\partial u_1}{\partial x_1})^3\rangle \times \langle(\frac{\partial u_1}{\partial x_1})^2\rangle^{1/2} \times R_\lambda^{-1.5} \sim \langle(\frac{\partial u_1}{\partial x_1})^2\rangle^2 R_\lambda^{-1.4} \sim \langle(\frac{\partial u_1}{\partial x_1})^4\rangle R_\lambda^{-1.7} \sim \langle(\overline{\mathbf{m}^2})^2\rangle R_\lambda^{-1.7}$, which is negligible when $R_\lambda \gg 1$.

For wall flows, Eq. (31) might not be applicable in the viscous sublayer, while we expect it to hold in and above the log-layer. In Fig. 3(a) we plot the ratio $-2\langle\overline{\mathbf{mh^p m}}\rangle/(\langle(\overline{\mathbf{m}^2})^2\rangle + 2\langle\overline{\mathbf{m}^2}m_{ij}\rangle M_{ji})$ vs y^+ in channel flows for two different Reynolds number $\mathrm{Re}_\tau = 1000$ and $\mathrm{Re}_\tau = 5200$. The data are downloaded from the data sets "channel flow" and "channel flow at $\mathrm{Re}_\tau = 5200$" in JHTDB [38,39]. The details of the simulations could be found in Refs. [38,39]. Briefly, in both simulations, the domain sizes are $8\pi \times 2 \times 3\pi$, using $2048 \times 512 \times 1536$ and $10240 \times 1536 \times 7680$ nodes, respectively, at the lower and higher Reynolds simulations. The Reynolds numbers based on the friction velocity at the wall u_τ, $\mathrm{Re}_\tau \equiv u_\tau h/\nu$ are 1000 and 5200 for these two flows, where h is the half-height of the channel and ν is the viscosity. In Fig. 3, for the $\mathrm{Re}_\tau = 1000$ simulation, we record data in 20 planes from the wall to the center of the channel, i.e., data in 20 positions from $y = 0$ to h, and in each plane we used 2.2×10^7 data points. And for the higher Reynolds number $\mathrm{Re}_\tau = 5200$, we record 26 planes, with 3.8×10^7 data points for each plane.

We can see from Fig. 3 that the ratio is close to the homogeneous value 1 when $y^+ > 10$, but significantly deviate from 1 in the near wall region: it increases as we move towards the wall, and reaches roughly 1.5 at $y^+ = 1$. For comparison, we also plot $-2\langle\overline{\mathbf{mh^p m}}\rangle/\langle(\overline{\mathbf{m}^2})^2\rangle$ in Fig. 3(b), it is clear that far from the wall, the curves in Fig. 3(b) deviate more from unity than the counterparts in Fig. 3(a) in the range $30 < y^+ < 1000$, suggesting a small but non-negligible contribution from $2\langle\overline{\mathbf{m}^2}m_{ij}\rangle M_{ji}$ in this range. To exclude the possible effects of statistical fluctuations on the small variations of those curves at about $y^+ = 100$, we check the statistical convergence by dividing the data points into several groups and compare their results with full statistics: the differences are no more than a few percent in the viscous sublayer, and negligible further away from the wall.
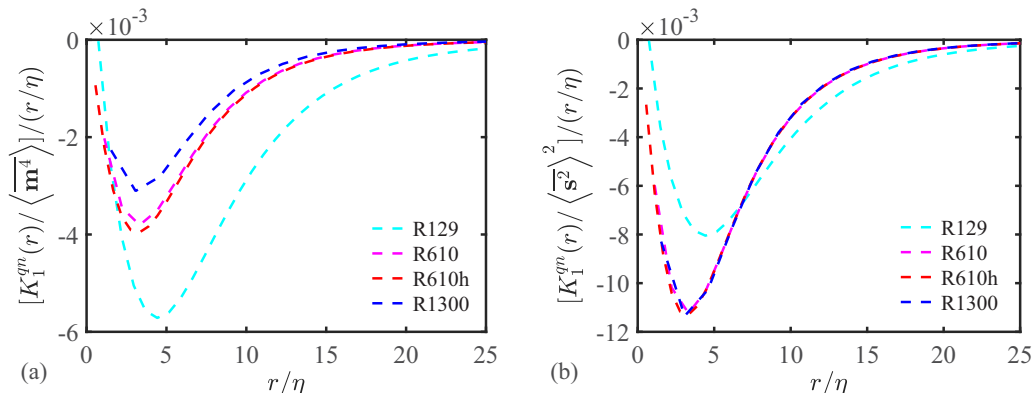
FIG. 4. $\frac{K_1^{qn}(r)}{r}$ normalized by (a) $\langle \overline{\mathbf{m}^4} \rangle/\eta$ and (b) $\langle \overline{\mathbf{s}^2} \rangle^2/\eta$ vs r/η. The cyan, magenta, red, and blue lines indicate cases R129, R610, R610h, and R1300, respectively.

VI. CONCLUDING REMARKS

In summary, we discussed the homogeneity constraint (12) to the mixed moment $\langle \overline{\mathbf{mh^p m}} \rangle$, which leads to various implications. Together with the Poisson equation for pressure Hessian [Eq. (15)], from Eq. (12) we can express $\langle \overline{\mathbf{mh^p m}} \rangle$ and thus $\langle (\overline{\mathbf{m}^2})^2 \rangle$ in terms of the integration of a two-point fourth-order velocity gradient correlation function. Then DNS results indicate that the integrand peaks at $\sim 3\eta$ and does not vary with the R_λ when it is high enough, thus although the mixed moment $\langle \overline{\mathbf{mh^p m}} \rangle$ is nonlocal as a result of the Poisson equation, it is still a dissipative scale quantity. Furthermore, Eq. (12) imposes a constraint on the closure model of pressure Hessian in the velocity gradient dynamics. Technically, plugging the model into Eq. (12) might generate an identity for the model parameters. As an example, we discuss the Gaussian closure model introduced in Ref. [14] and give a quantitative relation between the model parameters [Eq. (29)]. Equation (12) could also be generalized to homogeneous flows with mean gradient [see Eq. (31)]. Moreover, even in turbulent channel flows, which is a typical example of inhomogeneous turbulence, Eq. (31) is still approximately true in and above the log-layer.

In the future it would be interesting to analytically and numerically investigate the other independent mixed moments of pressure Hessian and velocity gradient, such as $\langle \overline{\mathbf{sh^p s}} \rangle$ and $\langle \boldsymbol{\omega} \cdot \mathbf{h^p} \cdot \boldsymbol{\omega} \rangle$. Also, the properties of mixed moments between pressure Hessian and velocity gradient could help us to develop better closure models of velocity gradient dynamics.

ACKNOWLEDGMENTS

APPENDIX A: DERIVATION OF THE FORMULAS BASED ON QUASINORMAL ASSUMPTION

In this Appendix, we first discuss the application of the q.n. assumption to the integration expression of $\langle \overline{\mathbf{mH^p m}} \rangle$, i.e., Eq. (16). Under the q.n. assumption, the integrand of Eq. (16), $\langle m_{ln} m_{nl}(0) m_{ij} m_{jk}(\mathbf{r}) \rangle$, splits to $2\langle m_{ln}(0) m_{ij}(\mathbf{r}) \rangle \langle m_{nl}(0) m_{jk}(\mathbf{r}) \rangle$, and similar operations could be applied to other fourth-order correlations like K_1 and K_2. In Fig. 4(a) we plot $\frac{K_1^{\text{q.n.}}(r)}{r}$ normalized by $\langle \overline{\mathbf{m}^4} \rangle/\eta$, where $K_1^{\text{q.n.}}(r)$ is the q.n. expression of $K_1(r)$: $K_1^{\text{q.n.}}(r) = 2\langle m_{ln}(0) m_{Lj}(\mathbf{r}) \rangle \langle m_{nl}(0) m_{jL}(\mathbf{r}) \rangle - 2\langle m_{ln}(0) m_{Nj}(\mathbf{r}) \rangle \langle m_{nl}(0) m_{jN}(\mathbf{r}) \rangle$. Compared with Fig. 1(b), although the values of those curves in

Fig. 4 are much smaller, they still catch the shape, and peak at $\sim 3\eta$. We should point out that $\langle \overline{\mathbf{m}^4} \rangle$ is not a proper normalization for $K_1^{qn}(r)$, which is the products of second-order correlations, thus as an alternative, in Fig. 4(b) we normalize $\frac{K_1^{\text{q.n.}}(r)}{r}$ by $\langle \overline{\mathbf{s}^2} \rangle^2 / \eta$. Again as in Fig. 1(b), the three curves with higher Reynolds number collapse very well, while the lower Reynolds number $R_\lambda = 129$ case shows some deviation.

Next, we calculate the q.n. value of $\langle m_{ij}m_{jk}H_{ki}^p \rangle$ by applying the q.n. assumption to the right-hand side of Eq. (16), which yields

$$
\begin{aligned}
\langle m_{ij}m_{jk}H_{ki}^p \rangle &= \frac{1}{4\pi} \int d\mathbf{r} \left[\frac{\delta_{ki}}{r^3} - 3\frac{r_i r_k}{r^5} \right] \langle m_{ln}m_{nl}(0)m_{ij}m_{jk}(\mathbf{r}) \rangle \\
&\overset{\text{q.n.}}{=} \frac{1}{4\pi} \int d\mathbf{r} \left[\frac{\delta_{ki}}{r^3} - 3\frac{r_i r_k}{r^5} \right] 2 \langle m_{ln}(0)m_{ij}(\mathbf{r}) \rangle \langle m_{nl}(0)m_{jk}(\mathbf{r}) \rangle.
\end{aligned}
\tag{A1}
$$

Notice that in isotropic flows, the fourth-rank tensor $T_{ijkl} \equiv \langle m_{ij}(0)m_{kl}(\mathbf{r}) \rangle$ could be expressed as the following:

$$
\begin{aligned}
T_{ijkl} = \langle m_{ij}(0)m_{kl}(\mathbf{r}) \rangle = {}& C_1 r_i r_j r_k r_l + C_2 r_i r_j \delta_{kl} + C_3 r_i r_k \delta_{jl} + C_4 r_i r_l \delta_{kj} + C_5 r_k r_l \delta_{ij} \\
& + C_6 r_j r_l \delta_{ik} + C_7 r_k r_j \delta_{il} + C_8 \delta_{ij}\delta_{kl} + C_9 \delta_{ik}\delta_{jl} + C_{10}\delta_{il}\delta_{kj}.
\end{aligned}
\tag{A2}
$$

Furthermore, one could readily see that

$$
T_{ijkl} = -\frac{\partial}{\partial r_j} \frac{\partial}{\partial r_l} Q_{ik}(\mathbf{r}),
\tag{A3}
$$

where the second-rank tensor Q_{ij} denotes the second-order velocity correlation $Q_{ij} = \langle u_i(0)u_j(\mathbf{r}) \rangle$, which has the following form under the isotropic condition:

$$
Q_{ij}(\mathbf{r}) = g(r)\delta_{ij} + [f(r) - g(r)]\frac{r_i r_j}{r^2},
\tag{A4}
$$

where $f(r)$ is the longitudinal correlation function $f(r) = Q_{LL}(r\hat{e}_L)$, and $g(r)$ is the transverse correlation function $g(r) = Q_{NN}(r\hat{e}_L)$, $\hat{e}_L$ denotes the normal direction of $\mathbf{r}$. Functions g and f satisfy the following identity due to the incompressible condition: $g(r) = f(r) + f'(r)r/2$, where $'$ denotes the derivative with respect to r. Then, plugging Eq. (A4) into Eq. (A3) yields

$$
\begin{aligned}
&C_1 = \frac{f'' - g''}{r^4} - 5\frac{f' - g'}{r^5} + 8\frac{f - g}{r^6}, \quad C_2 = C_3 = C_4 = C_5 = C_7 = \frac{f' - g'}{r^3} - 2\frac{f - g}{r^4}, \\
&C_6 = \frac{g''}{r^2} - \frac{g'}{r^3}, \quad C_9 = \frac{g'}{r}, \quad C_8 = C_{10} = \frac{f - g}{r^2}.
\end{aligned}
\tag{A5}
$$

Therefore, we have

$$
\begin{aligned}
\langle m_{ij}m_{jk}H_{ki}^p \rangle &\overset{\text{q.n.}}{=} \frac{1}{4\pi} \int d\mathbf{r} \left[\frac{\delta_{ki}}{r^3} - 3\frac{r_i r_k}{r^5} \right] 2 T_{lnij} T_{nljk} \\
&= 2 \int_0^\infty dr \frac{-2(f'')^2 r^2 + f'f'''r^2 - 4f'f''r + 6(f')^2}{r^3} \\
&= 2 \int_0^\infty dr \left(\frac{-2f'f''}{r} - \frac{3(f')^2}{r^2} \right)' = 2 \left. \left(\frac{2f'f''}{r} + \frac{3(f')^2}{r^2} \right) \right|_{r=0}.
\end{aligned}
\tag{A6}
$$

Notice that at small r, function f can be Taylor expanded as $f(r) \sim u'^2 - \frac{\varepsilon}{30\nu}r^2 = u'^2 - \frac{\langle \overline{\mathbf{s}^2} \rangle}{15}r^2$, thus,

$f'(r)/r|_{r=0} = f''(0) = -\frac{2}{15}\langle \overline{\mathbf{s}^2} \rangle$. Therefore, $\langle m_{ij}m_{jk}H_{ki}^p \rangle \overset{\text{q.n.}}{=} 2(\frac{2f'f''}{r} + \frac{3(f')^2}{r^2})|_{r=0} = \frac{8}{45}\langle \overline{\mathbf{s}^2} \rangle^2$. As a self-consistency check, we show that the q.n. value of the left-hand side of Eq. (24) also equals

TABLE IV. Quasinormal predictions for invariants I's and $\langle \omega_i \omega_j H_{ij}^p \rangle$, $\langle s_{ij} s_{jk} H_{ki}^p \rangle$ normalized by $\langle \overline{\mathbf{s}^2} \rangle^2$.

	I_1	I_2	I_3	I_4	$\langle \omega_i \omega_j H_{ij}^p \rangle$	$\langle s_{ij} s_{jk} H_{ki}^p \rangle$
q.n. predictions	$\frac{7}{5}$	2	$\frac{2}{3}$	$\frac{20}{3}$	$\frac{4}{9}$	$\frac{1}{15}$

to $\frac{8}{45} \langle \overline{\mathbf{s}^2} \rangle^2$. Applying the q.n. assumption, the left-hand side of Eq. (24) reads as

$$\frac{1}{6} \langle (m_{ij} m_{ji})^2 \rangle = \frac{1}{6} \left\langle \frac{\partial u_i}{\partial x_j} \frac{\partial u_j}{\partial x_i} \frac{\partial u_m}{\partial x_n} \frac{\partial u_n}{\partial x_m} \right\rangle \overset{\text{q.n.}}{=} \frac{1}{3} \left\langle \frac{\partial u_i}{\partial x_j} \frac{\partial u_m}{\partial x_n} \right\rangle \left\langle \frac{\partial u_j}{\partial x_i} \frac{\partial u_n}{\partial x_m} \right\rangle. \tag{A7}$$

Then notice that for homogeneous and isotropic turbulence, the second-order moments of velocity gradient have the following general expression:

$$\left\langle \frac{\partial u_i}{\partial x_j} \frac{\partial u_k}{\partial x_l} \right\rangle = \beta \left(\delta_{ik} \delta_{jl} - \frac{1}{4} \delta_{ij} \delta_{kl} - \frac{1}{4} \delta_{il} \delta_{jk} \right), \tag{A8}$$

where $\beta = 2\varepsilon/15\nu = \frac{4}{15} \langle \overline{\mathbf{s}^2} \rangle$. Thus,

$$\begin{aligned}
\frac{1}{6} \langle (m_{ij} m_{ji})^2 \rangle &\overset{\text{q.n.}}{=} \frac{1}{3} \left\langle \frac{\partial u_i}{\partial x_j} \frac{\partial u_m}{\partial x_n} \right\rangle \left\langle \frac{\partial u_j}{\partial x_i} \frac{\partial u_n}{\partial x_m} \right\rangle \\
&= \frac{\beta^2}{3} \left(\delta_{im} \delta_{jn} - \frac{1}{4} \delta_{ij} \delta_{mn} - \frac{1}{4} \delta_{in} \delta_{jm} \right) \left(\delta_{jn} \delta_{im} - \frac{1}{4} \delta_{ji} \delta_{nm} - \frac{1}{4} \delta_{jm} \delta_{in} \right) \\
&= \frac{5}{2} \beta^2 = \frac{8}{45} \langle \overline{\mathbf{s}^2} \rangle^2.
\end{aligned} \tag{A9}$$

Incidentally, parallel to the above derivation, we could also evaluate the value of $\langle s_{ij} s_{jk} H_{ki}^p \rangle$ within the q.n. formalism:

$$\begin{aligned}
\langle s_{ij} s_{jk} H_{ki}^p \rangle &\overset{\text{q.n.}}{=} \frac{1}{4\pi} \int d\mathbf{r} \left[\frac{\delta_{ki}}{r^3} - 3 \frac{r_i r_k}{r^5} \right] (2 T_{lnij} T_{nljk} + T_{lnji} T_{nljk} + T_{lnij} T_{nlkj}) \\
&= \int_0^\infty d\mathbf{r} \frac{2 f' f'' r + f'' f''' r^3/2 - 2(f')^2}{r^3} \\
&= \int_0^\infty d\mathbf{r} \left(\frac{-2 f' f''}{r} - \frac{3(f')^2}{r^2} + \frac{(f')^2}{r^2} + \frac{(f'')^2}{4} \right)' = \frac{1}{15} \langle \overline{\mathbf{s}^2} \rangle^2
\end{aligned} \tag{A10}$$

and similar calculation leads to $\langle \omega_i \omega_j H_{ij}^p \rangle \overset{\text{q.n.}}{=} \frac{4}{9} \langle \overline{\mathbf{s}^2} \rangle^2$. In Table IV we summarize the q.n. predictions for fourth-order invariants I_1 to I_4 [5] and mixed moments $\langle s_{ij} s_{jk} H_{ki}^p \rangle$, $\langle \omega_i \omega_j H_{ij}^p \rangle$ normalized by $\langle \overline{\mathbf{s}^2} \rangle^2$.

Under the Gaussian closure model (27) proposed in Ref. [14], similar to Eq. (28), one could readily show that

$$\langle s_{ij} s_{jk} H_{ki}^p \rangle = -\frac{\alpha}{6} I_1 + \frac{\beta}{12} I_2 - \frac{\beta}{4} I_3 \tag{A11}$$

and

$$\langle w_{ij} w_{jk} H_{ki}^p \rangle = \frac{\alpha}{12} I_2 - \frac{\alpha}{4} I_3 - \frac{\beta}{24} I_4. \tag{A12}$$

With $\alpha = -\frac{2}{7}$ and $\beta = -\frac{2}{5}$, Eqs. (A11) and (A12) are consistent with Table IV under the q.n. assumption.

TABLE V. DNS results for the six-order moments $\langle(\overline{\mathbf{m}^2})^3\rangle$ and the related mixed moments between velocity gradient and pressure Hessian. All quantities in the table are normalized by $\langle\overline{\mathbf{s}^2}\rangle^3$. We list the results from case R610h of HIT here since this data set has the largest resolution.

$\langle\overline{\mathbf{h}^\mathbf{p}}\,\overline{\mathbf{h}^\mathbf{p}\mathbf{m}^2}\rangle$	$\langle\overline{\mathbf{h}^{\mathbf{p}2}}\,\overline{\mathbf{m}^2}\rangle$	$\langle\overline{\mathbf{h}^\mathbf{p}\mathbf{m}^2}\rangle$	$\langle\overline{\mathbf{h}^{\mathbf{p}2}}\,\overline{\mathbf{m}^2}\rangle$	$\langle(\overline{\mathbf{m}^2})^3\rangle$	$\langle\overline{\mathbf{h}^{\mathbf{p}2}\mathbf{m}^2}\rangle$
-120.6	-121.1	4.648	-241.9		-61.81
$\langle(\overline{\mathbf{h}^\mathbf{p}\mathbf{m}})^2\rangle$	$\langle\overline{\mathbf{H}^{\mathbf{p}2}}\,\overline{\mathbf{m}^2}\rangle$	$\langle\overline{\mathbf{H}^\mathbf{p}\mathbf{m}^2}\rangle$	$\langle\overline{\mathbf{H}^{\mathbf{p}2}\mathbf{m}^2}\rangle$		$\langle(\overline{\mathbf{H}^\mathbf{p}\mathbf{m}})^2\rangle$
-52.55	-40.58	4.649	-8.299		0.9535

APPENDIX B: FOURTH-ORDER INVARIANTS RELATIONS

The derivation of Eq. (8) only requires chain rule of derivatives and homogeneity condition [22]. A natural question is whether this derivation could be generalized to higher-order moments. Here we discuss the $n = 4$ case. Similar to the derivation of Eq. (8), one could show that four different vector gradient fields $\mathbf{h}^\mathbf{a} = \nabla\mathbf{a}$, $\mathbf{h}^\mathbf{b} = \nabla\mathbf{b}$, $\mathbf{h}^\mathbf{c} = \nabla\mathbf{c}$, and $\mathbf{h}^\mathbf{d} = \nabla\mathbf{d}$ satisfy the following relation:

$$\langle\overline{\mathbf{h}^\mathbf{a}}\,\overline{\mathbf{h}^\mathbf{b}}\,\overline{\mathbf{h}^\mathbf{c}}\,\overline{\mathbf{h}^\mathbf{d}}\rangle + \langle\overline{\mathbf{h}^\mathbf{a}}\,\overline{\mathbf{h}^\mathbf{b}\mathbf{h}^\mathbf{c}\mathbf{h}^\mathbf{d}}\rangle + \langle\overline{\mathbf{h}^\mathbf{a}}\,\overline{\mathbf{h}^\mathbf{b}\mathbf{h}^\mathbf{d}\mathbf{h}^\mathbf{c}}\rangle + \langle\overline{\mathbf{h}^\mathbf{b}}\,\overline{\mathbf{h}^\mathbf{a}\mathbf{h}^\mathbf{c}\mathbf{h}^\mathbf{d}}\rangle + \langle\overline{\mathbf{h}^\mathbf{b}}\,\overline{\mathbf{h}^\mathbf{a}\mathbf{h}^\mathbf{d}\mathbf{h}^\mathbf{c}}\rangle + \langle\overline{\mathbf{h}^\mathbf{c}}\,\overline{\mathbf{h}^\mathbf{a}\mathbf{h}^\mathbf{b}\mathbf{h}^\mathbf{d}}\rangle$$
$$+ \langle\overline{\mathbf{h}^\mathbf{c}}\,\overline{\mathbf{h}^\mathbf{a}\mathbf{h}^\mathbf{d}\mathbf{h}^\mathbf{b}}\rangle + \langle\overline{\mathbf{h}^\mathbf{d}}\,\overline{\mathbf{h}^\mathbf{a}\mathbf{h}^\mathbf{b}\mathbf{h}^\mathbf{c}}\rangle + \langle\overline{\mathbf{h}^\mathbf{d}}\,\overline{\mathbf{h}^\mathbf{a}\mathbf{h}^\mathbf{c}\mathbf{h}^\mathbf{b}}\rangle + \langle\overline{\mathbf{h}^\mathbf{a}\mathbf{h}^\mathbf{b}}\,\overline{\mathbf{h}^\mathbf{c}\mathbf{h}^\mathbf{d}}\rangle + \langle\overline{\mathbf{h}^\mathbf{a}\mathbf{h}^\mathbf{c}}\,\overline{\mathbf{h}^\mathbf{b}\mathbf{h}^\mathbf{d}}\rangle + \langle\overline{\mathbf{h}^\mathbf{a}\mathbf{h}^\mathbf{d}}\,\overline{\mathbf{h}^\mathbf{b}\mathbf{h}^\mathbf{c}}\rangle$$
$$= \langle\overline{\mathbf{h}^\mathbf{a}}\,\overline{\mathbf{h}^\mathbf{b}}\,\overline{\mathbf{h}^\mathbf{c}\mathbf{h}^\mathbf{d}}\rangle + \langle\overline{\mathbf{h}^\mathbf{a}}\,\overline{\mathbf{h}^\mathbf{c}}\,\overline{\mathbf{h}^\mathbf{b}\mathbf{h}^\mathbf{d}}\rangle + \langle\overline{\mathbf{h}^\mathbf{a}}\,\overline{\mathbf{h}^\mathbf{d}}\,\overline{\mathbf{h}^\mathbf{b}\mathbf{h}^\mathbf{c}}\rangle + \langle\overline{\mathbf{h}^\mathbf{b}}\,\overline{\mathbf{h}^\mathbf{c}}\,\overline{\mathbf{h}^\mathbf{a}\mathbf{h}^\mathbf{d}}\rangle + \langle\overline{\mathbf{h}^\mathbf{b}}\,\overline{\mathbf{h}^\mathbf{d}}\,\overline{\mathbf{h}^\mathbf{a}\mathbf{h}^\mathbf{c}}\rangle + \langle\overline{\mathbf{h}^\mathbf{c}}\,\overline{\mathbf{h}^\mathbf{d}}\,\overline{\mathbf{h}^\mathbf{a}\mathbf{h}^\mathbf{b}}\rangle$$
$$+ \langle\overline{\mathbf{h}^\mathbf{a}\mathbf{h}^\mathbf{b}\mathbf{h}^\mathbf{c}\mathbf{h}^\mathbf{d}}\rangle + \langle\overline{\mathbf{h}^\mathbf{a}\mathbf{h}^\mathbf{b}\mathbf{h}^\mathbf{d}\mathbf{h}^\mathbf{c}}\rangle + \langle\overline{\mathbf{h}^\mathbf{a}\mathbf{h}^\mathbf{c}\mathbf{h}^\mathbf{b}\mathbf{h}^\mathbf{d}}\rangle + \langle\overline{\mathbf{h}^\mathbf{a}\mathbf{h}^\mathbf{c}\mathbf{h}^\mathbf{d}\mathbf{h}^\mathbf{b}}\rangle + \langle\overline{\mathbf{h}^\mathbf{a}\mathbf{h}^\mathbf{d}\mathbf{h}^\mathbf{b}\mathbf{h}^\mathbf{c}}\rangle + \langle\overline{\mathbf{h}^\mathbf{a}\mathbf{h}^\mathbf{d}\mathbf{h}^\mathbf{c}\mathbf{h}^\mathbf{b}}\rangle.$$
$$(B1)$$

However, this relation does not provide an additional constraint from homogeneity. Tensor analysis shows that any three second-order tensors $\mathbf{A}$, $\mathbf{B}$, and $\mathbf{C}$ satisfy the following three-dimensional Rivlin's identities [cf. Eq. (6.163) of Ref. [40]]:

$$\mathbf{ABC} + \mathbf{ACB} + \mathbf{BCA} + \mathbf{BAC} + \mathbf{CAB} + \mathbf{CBA} + \mathbf{A}\overline{\mathbf{B}}\,\overline{\mathbf{C}} + \mathbf{B}\overline{\mathbf{A}}\,\overline{\mathbf{C}} + \mathbf{C}\overline{\mathbf{A}}\,\overline{\mathbf{B}} + (\overline{\mathbf{A}}\,\overline{\mathbf{BC}} + \overline{\mathbf{B}}\,\overline{\mathbf{AC}} + \overline{\mathbf{C}}\,\overline{\mathbf{AB}})\mathbf{I}$$
$$= \overline{\mathbf{A}}(\mathbf{BC} + \mathbf{CB}) + \overline{\mathbf{B}}(\mathbf{AC} + \mathbf{CA}) + \overline{\mathbf{C}}(\mathbf{AB} + \mathbf{BA}) + \mathbf{A}\overline{\mathbf{BC}} + \mathbf{B}\overline{\mathbf{AC}} + \mathbf{C}\overline{\mathbf{AB}}$$
$$+ (\overline{\mathbf{A}}\,\overline{\mathbf{B}}\,\overline{\mathbf{C}} + \overline{\mathbf{ABC}} + \overline{\mathbf{ACB}})\mathbf{I},$$
$$(B2)$$

where $\mathbf{I}$ denotes the identity matrix. Now choosing $\mathbf{A} = \mathbf{h}^\mathbf{a}$, $\mathbf{B} = \mathbf{h}^\mathbf{b}$, and $\mathbf{C} = \mathbf{h}^\mathbf{c}$ in Eq. (B2), then multiplying Eq. (B2) with $\mathbf{h}^\mathbf{d}$ and taking the trace, one could exactly recover Eq. (B1). To numerically examine Eq. (B1), we choose $\mathbf{h}^\mathbf{a} = \mathbf{h}^\mathbf{b} = \mathbf{h}^\mathbf{p}$ and $\mathbf{h}^\mathbf{c} = \mathbf{h}^\mathbf{d} = \mathbf{m}$ in Eq. (B1) as an example, which yields

$$4\langle\overline{\mathbf{h}^\mathbf{p}}\,\overline{\mathbf{h}^\mathbf{p}\mathbf{m}^2}\rangle + \langle\overline{\mathbf{h}^{\mathbf{p}2}}\,\overline{\mathbf{m}^2}\rangle + 2\langle\overline{\mathbf{h}^\mathbf{p}\mathbf{m}^2}\rangle = \langle\overline{\mathbf{h}^{\mathbf{p}2}}\,\overline{\mathbf{m}^2}\rangle + 4\langle\overline{\mathbf{h}^{\mathbf{p}2}\mathbf{m}^2}\rangle + 2\langle(\overline{\mathbf{h}^\mathbf{p}\mathbf{m}})^2\rangle, \qquad (B3)$$

this equation could also be expressed in terms of $\mathbf{H}^\mathbf{p}$:

$$\langle\overline{\mathbf{H}^{\mathbf{p}2}}\,\overline{\mathbf{m}^2}\rangle + 2\langle\overline{\mathbf{H}^\mathbf{p}\mathbf{m}^2}\rangle = 4\langle\overline{\mathbf{H}^{\mathbf{p}2}\mathbf{m}^2}\rangle + 2\langle(\overline{\mathbf{H}^\mathbf{p}\mathbf{m}})^2\rangle. \qquad (B4)$$

In Table V we list the DNS results for those quantities appearing in Eqs. (B3) and (B4). We can see that the data agree well with Eqs. (B3) and (B4).

[1] R. Betchov, An inequality concerning the production of vorticity in isotropic turbulence, J. Fluid Mech. **1**, 497 (1956).

[2] W. T. Ashurst, A. R. Kerstein, R. M. Kerr, and C. H. Gibson, Alignment of vorticity and scalar gradient with strain rate in simulated Navier-Stokes turbulence, Phys. Fluids **30**, 2343 (1987).

[3] C. Meneveau, Lagrangian dynamics and models of the velocity gradient tensor in turbulent flows, Annu. Rev. Fluid Mech. **43**, 219 (2011).

[4] A. Tsinober, *An Informal Conceptual Introduction to Turbulence* (Springer, Berlin, 2009).

[5] E. D. Siggia, Invariants for the onepoint vorticity and strain rate correlation functions, Phys. Fluids **24**, 1934 (1981).

[6] J. Hierro and C. Dopazo, Fourth-order statistical moments of the velocity gradient tensor in homogeneous, isotropic turbulence, Phys. Fluids **15**, 3434 (2003).

[7] R. M. Kerr, Higher-order derivative correlations and the alignment of small-scale structures in isotropic numerical turbulence, J. Fluid Mech. **153**, 31 (1985).

[8] T. Ishihara, Y. Kaneda, M. Yokokawa, K. Itakura, and A. Uno, Small-scale statistics in high-resolution direct numerical simulation of turbulence: Reynolds number dependence of one-point velocity gradient statistics, J. Fluid Mech. **592**, 335 (2007).

[9] L. Fang, Y. J. Zhang, J. Fang, and Y. Zhu, Relation of the fourth-order statistical invariants of velocity gradient tensor in isotropic turbulence, Phys. Rev. E **94**, 023114 (2016).

[10] L. Djenidi, L. Danaila, R. A. Antonia, and S. Tang, A note on the velocity derivative flatness factor in decaying HIT, Phys. Fluids **29**, 051702 (2017).

[11] S. L. Tang, R. A. Antonia, L. Djenidi, L. Danaila, and Y. Zhou, Reappraisal of the velocity derivative flatness factor in various turbulent flows, J. Fluid Mech. **847**, 244 (2018).

[12] J. Boschung, Exact relations between the moments of dissipation and longitudinal velocity derivatives in turbulent flows, Phys. Rev. E **92**, 043013 (2015).

[13] L. Chevillard, C. Meneveau, L. Biferale, and F. Toschi, Modeling the pressure Hessian and viscous Laplacian in turbulence: Comparisons with direct numerical simulation and implications on velocity gradient dynamics, Phys. Fluids **20**, 101504 (2008).

[14] M. Wilczek and C. Meneveau, Pressure Hessian and viscous contributions to velocity gradient statistics based on Gaussian random fields, J. Fluid Mech. **756**, 191 (2014).

[15] J. M. Lawson and J. R. Dawson, On velocity gradient dynamics and turbulent structure, J. Fluid Mech. **780**, 60 (2015).

[16] M. Carbone, M. Iovieno, and A. D. Bragg, Symmetry transformation and dimensionality reduction of the anisotropic pressure Hessian, J. Fluid Mech. **900**, A38 (2020).

[17] J. Tom, M. Carbone, and A. D. Bragg, Exploring the turbulent velocity gradients at different scales from the perspective of the strain-rate eigenframe, J. Fluid Mech. **910**, A24 (2021).

[18] D. G. Vlaykov and M. Wilczek, On the small-scale structure of turbulence and its impact on the pressure field, J. Fluid Mech. **861**, 422 (2019).

[19] A. Tsinober, M. Ortenberg, and L. Shtilman, On depression of nonlinearity in turbulence, Phys. Fluids **11**, 2291 (1999).

[20] M. Carbone and M. Wilczek, Only two Betchov homogeneity constraints exist for isotropic turbulence, J. Fluid Mech. **948**, R2 (2022).

[21] B. J. Cantwell, Exact solution of a restricted Euler equation for the velocity gradient tensor, Phys. Fluids **4**, 782 (1992).

[22] P.-F. Yang, J. Fang, L. Fang, A. Pumir, and H. Xu, Low-order moments of the velocity gradient in homogeneous compressible turbulence, J. Fluid Mech. **947**, R1 (2022).

[23] Z. D. Zhou, S. Z. Wang, and G. D. Jin, A structural subgrid-scale model for relative dispersion in large-eddy simulation of isotropic turbulent flows by coupling kinematic simulation with approximate deconvolution method, Phys. Fluids **30**, 105110 (2018).

[24] Z. D. Zhou, G. W. He, S. Z. Wang, and G. D. Jin, Subgrid-scale model for Large-Eddy simulation of isotropic turbulent flows using an artificial neural network, Comput. Fluids **195**, 104319 (2019).

[25] Y. Li, E. Perlman, M. Wan, Y. Yang, C. Meneveau, R. Burns, S. Chen, A. Szalay, and G. L. Eyink, A public turbulence database cluster and applications to study Lagrangian evolution of velocity increments in turbulence, J. Turbul. **9**, 1 (2008).

[26] P. K. Yeung, D. A. Donzis, and K. R. Sreenivasan, Dissipation, enstrophy and pressure statistics in turbulence simulations at high Reynolds numbers, J. Fluid Mech. **700**, 5 (2012).

[27] P. K. Yeung, X. M. Zhai, and K. R. Sreenivasan, Extreme events in computational turbulence, Proc. Natl. Acad. Sci. USA **112**, 12633 (2015).

[28] P. K. Yeung, K. R. Sreenivasan, and S. B. Pope, Effects of finite spatial and temporal resolution on extreme events in direct numerical simulations of incompressible isotropic turbulence, Phys. Rev. Fluids **3**, 064603 (2018).

[29] K. Ohkitani and S. Kishiba, Nonlocal nature of vortex stretching in an inviscid fluid, Phys. Fluids **7**, 411 (1995).

[30] A. J. Majda and A. L. Bertozzi, *Vorticity and Incompressible Flow* (Cambridge University Press, Cambridge, 2002).

[31] V. Borue and S. A. Orszag, Local energy flux and subgrid-scale statistics in three-dimensional turbulence, J. Fluid Mech. **366**, 1 (1998).

[32] M. Chertkov, A. Pumir, and B. I. Shraiman, Lagrangian tetrad dynamics and the phenomenology of turbulence, Phys. Fluids **11**, 2394 (1999).

[33] L. A. Leppin and M. Wilczek, Capturing Velocity Gradients and Particle Rotation Rates in Turbulence, Phys. Rev. Lett. **125**, 224501 (2020).

[34] P. Bradshaw and J. B. Perot, A note on turbulent energy dissipation in the viscous wall region, Phys. Fluids **5**, 3305 (1993).

[35] A. Pumir, H. Xu, and E. D. Siggia, Small-scale anisotropy in turbulent boundary layers, J. Fluid Mech. **804**, 5 (2016).

[36] A. Pumir, Structure of the velocity gradient tensor in turbulent shear flows, Phys. Rev. Fluids **2**, 074602 (2017).

[37] S. B. Pope, *Turbulent Flows* (Cambridge University Press, Cambridge, 2000).

[38] J. Graham, K. Kanov, X. I. A. Yang, M. Lee, N. Malaya, C. C. Lalescu, R. Burns, G. Eyink, A. Szalay, R. D. Moser, and C. Meneveau, A web services accessible database of turbulent channel flow and its use for testing a new integral wall model for LES, J. Turbul. **17**, 181 (2016).

[39] M. Lee and R. D. Moser, Small-scale anisotropy in turbulent boundary layers, J. Fluid Mech. **774**, 395 (2015).

[40] M. Itskov, *Tensor Algebra and Tensor Analysis for Engineers* (Springer, Cham, 2015).